

Ionospheric control of space weather

Osuke Saka

Office Geophysik, Ogoori, 838-0141, Japan

Abstract

As proposed by Saka (2019), plasma injections arising out of the auroral ionosphere (ionospheric injection) are a characteristic process of the polar ionosphere at substorm onset. The ionospheric injection is triggered by westward electric fields transmitted from the convection surge in the magnetosphere at field line dipolarization. Localized westward electric fields result in local accumulation of ionospheric electrons/ions which produce local electrostatic potentials in the auroral ionosphere. Field-aligned electric fields are developed to extract excess charges from the ionosphere. This process is essential to equipotential equilibrium of the auroral ionosphere. Cold electrons/ions that evaporate from the auroral ionosphere by ionospheric injection tend to generate electrostatic parallel potential below an altitude of 10,000 km. This is a result of charge separation along the mirror fields introduced by the evaporated electrons and ions moving earthward in phase space.

1. Introduction

Discontinuous reconfigurations of geomagnetic fields, referred to as field line dipolarization, are a significant geomagnetic event at substorm onset. Various causes have been suggested, most notably: the formation of X-points [Baker, et al., 1996]; flow braking [Birn et al., 1999]; local enhancement of plasma pressures [Tanaka et al., 2010]; arrival of plasma bubbles [Birn et al., 2004]; plasma instabilities [McPherron et al., 1973; Roux et al., 1991; Lui, 1996; Liu and Liang, 2009]; and relaxation of radial inhomogeneity [Saka, 2020]. Field line dipolarization alters global current circuits in the midnight magnetosphere thereby dipolarizing geomagnetic field lines [McPherron et al., 1973].

Field line dipolarization invokes inductive westward electric fields at the equatorial plane with the arrival of Dipolarization Front [Runov et al., 2011; Liu et al., 2014]. These fields penetrate the polar ionosphere and yield plasma injections from the ionosphere (ionospheric injection) with associated nonlinear evolution of the plasma motions [Saka, 2019]. This development

37 in turn leads to poleward expansion of auroras [e.g., Nielsen and Greenwald, 1978] and
38 vertical flows of ionospheric plasmas [e.g., Wahlund et al., 1992]. Ionospheric injection can
39 be regarded as an evaporation of ionospheric plasmas into the magnetosphere. This report
40 focuses on how this evaporation process builds up parallel potentials in higher altitudes
41 above the ionosphere to initiate auroral onset.

42 In Section 2, ionospheric injection scenario associated with field line dipolarization is briefly
43 described. In Section 3, development of parallel potentials in the flux tubes is explained.
44 Section 4 discusses polarity and intensity of field-aligned currents in parallel potentials. In
45 Section 5, ionospheric injection scenario is summarized within the context of the coupling
46 process of the magnetosphere and ionosphere.

47

48 *2. Ionospheric injection*

49 The ionospheric injection scenario proposed in Saka [2019] is as follows: (1) External electric
50 fields penetrated in the polar ionosphere produce local accumulation/rarefaction of electric
51 charges in the E-layer by the mobility difference of electrons and ions; (2) Resulting charge
52 separation may be readily reduced by the secondary (polarization) electric fields; (3) A
53 fraction of particle populations is released out of the ionosphere as ionospheric injections to
54 sustain initial potential distributions in quasi-neutral equilibrium.

55 This ionospheric injection scenario is schematically shown in Figure 1. Ionospheric injection
56 results in both generator and load. Localized westward electric fields (\mathbf{E}_w) accumulated
57 negative charges (electrons) in lower latitudes leaving positive charges (ions) in higher
58 latitudes because of differing electron and ion mobility in the E-layer (blue arrow, generator).

59 Polarization electric fields (\mathbf{E}_p) produced by the charge separation moved ions to lower

60 latitudes ($\mathbf{U}_{i\perp} = b_i \mathbf{E}_p$, b_i is mobility of ions) as Pedersen currents to neutralize the
61 ionosphere (red arrow, load). To avoid a complete neutralization of the ionosphere, some
62 positive charges (ions) in negative potential regions in lower latitudes and some negative
63 charges (electrons) in positive potential regions in higher latitudes were expelled from the
64 ionosphere. This partial neutralization process sustained original potential distributions in
65 quasi-neutral equilibrium. In Figure 1, we do not include the Hall currents driven by the
66 secondary polarization electric fields. The Hall current produce current vortices flowing
67 clockwise (as viewed from above) in a positive potential region in higher latitudes and
68 counterclockwise in negative potentials in lower latitudes.

69 Meanwhile, geomagnetic field lines are not in equipotential equilibrium during ionospheric

70 injections but instead develop both downward electric fields in positive potential regions of
 71 higher latitudes to extract electrons located there and upward electric fields in negative
 72 potential regions of lower latitudes to extract ions. Ionospheric injection is an evaporation
 73 process of ionospheric electrons and ions along the flux tubes at the substorm onset.

74

75 *3. Development of parallel potentials*

76 For about 10 minutes following Pi2 onset, nighttime magnetosphere could be in a transitional
 77 state repeating local field line dipolarization [Saka et al., 2010]. In this transitional interval,
 78 steady-state motions of electrons and ions can be assumed. In guiding center approximation,
 79 one-dimensional parallel motion could be given as,

$$80 \quad v_{\parallel} \frac{\partial v_{\parallel}}{\partial s} = G_{\parallel} + \frac{q|e|}{m_q} E_{\parallel} - \frac{\mu_q}{m_q} \frac{\partial B}{\partial s} \quad (1)$$

81 In equation (1), $|e|$ is the charge, m_q is the mass, μ_q is the magnetic moment, G_{\parallel} is
 82 the gravitational acceleration, B is the magnetic field strength, E_{\parallel} is the parallel electric
 83 field, v_{\parallel} is the parallel velocity, and s is along field lines. Note that $q=1$ for ions and
 84 $q=-1$ for electrons. In this equation, centrifugal force is ignored. Equation (1) can be
 85 reduced to the constants of the motion (W , μ),

$$86 \quad W = \frac{m_q}{2} (v_{\parallel}^2 + v_{\perp}^2) + q|e|\Phi \quad (2)$$

$$87 \quad \mu = \frac{m_q}{2B} v_{\perp}^2 \quad (3)$$

88 Here, v_{\perp} and Φ denote perpendicular velocity and electrostatic potential along the field
 89 lines, respectively.

90 Gravitational term in (1) can be ignored in (2) if the electrostatic potential above the
 91 ionosphere decreased below -10 Volt for ions.

92 Combination of equations (2) and (3) yields,

$$93 \quad v_{\parallel}^2 = v_{\parallel}^2 + (1 - B'/B)v_{\perp}^2 + (2q|e|/m_q)(\Phi - \Phi') \quad (4)$$

94 Equation (4) gives dynamical trajectory in phase space between two points, $(v_{\parallel}', v_{\perp}'; \Phi')$

95 and $(v_{//}, v_{\perp}; \Phi)$, along the same field lines [e.g., Chiu and Schulz, 1978].

96 If the dynamical trajectory starts from the bottom-side ionosphere, $(v'_{//}, v'_{\perp}; \Phi')$ is at the

97 ionospheric E-layer and $(v_{//}, v_{\perp}; \Phi)$ is either at 1,000km, 10,000 km, 20,000 km and at

98 geosynchronous (50,000 km) altitudes. The trajectory trace of the velocity space is shown in

99 Figures 2 and 3.

100 In Figure 2, both the magnetic mirror force and parallel potential accelerated ionospheric

101 sources. This acceleration process moved ionospheric source plasmas labelled (Σ) to the

102 bottom-right or to the bottom-left corner in velocity space as the altitudes increased from

103 1,000 km to the geosynchronous altitudes. Figure 2 illustrates two cases: (1) Ionospheric

104 electrons are accelerated in downward electric fields where field-aligned potential increased

105 with increasing altitudes; (2) Ionospheric ions are accelerated in upward electric fields where

106 the potential decreased with increasing altitudes. Assuming the Maxwell distribution function

107 for velocity distributions of ions and electrons above 1,000 km in altitudes, in accordance with

108 Liouville's theorem ($df/dt = 0$) we calculate parallel and perpendicular temperatures of

109 ionospheric species at altitudes of 1,000 km, 10,000 km, 20,000 km, and geosynchronous.

110 The velocity distribution function of ionospheric plasmas is given by,

$$111 \quad f(v_{//}, v_{\perp}; \Phi) = \left(\frac{m_q}{2\pi kT_q} \right)^{3/2} \exp \left(\frac{m_q}{2kT_q} (v_{//}^2 + v_{\perp}^2) + \frac{q|e|\Phi}{kT_q} \right) \quad (5)$$

112 Here kT_q is 1 eV for ions/electrons. Electrostatic potential Φ is 0 volt at the ionosphere.

113 The temperature of parallel/perpendicular component in eV is given by $\frac{m_q}{2} \langle v_{//,\perp}^2 \rangle$, where

$$114 \quad \langle v_{//,\perp}^2 \rangle = \frac{\int_{\Sigma} v_{//,\perp}^2 f(v) d^3v}{\int_{\Sigma} f(v) d^3v} \quad (6)$$

115 Integration was carried out over the velocity space (Σ) bounded by the hyperbolic curves,

116 both in negative (earthward) and positive (tailward) velocity component in $v_{//}$.

117 For both ions and electrons, parallel and perpendicular temperatures $\left(\frac{m_q}{2} \langle v_{//}^2 \rangle, \frac{m_q}{2} \langle v_{\perp}^2 \rangle \right)$

118 initially (0.5 eV, 1.0 eV) in the ionosphere changed to (11.3 eV, 0.70 eV) at 1,000 km where

119 electrostatic potential was 10 V for electrons and -10 V for ions. Temperatures changed to

120 (51.9 eV, 0.09 eV) at 10,000 km where electrostatic potential was 50 V for electrons and -50
121 V for ions. When electrostatic potential further increased to 200 V for electrons and
122 decreased to -200 V for ions at 20,000 km, temperatures changed to (202.0 eV, 0.02 eV). At
123 geosynchronous altitudes, temperatures changed to (502 eV, 0.002 eV) where potential is
124 assumed to be 500 V for electrons and -500 V for ions. Parallel potential and mirror geometry
125 skewed velocity space of the ionospheric source and increased parallel temperatures and
126 decreased perpendicular ones at altitudes above the ionosphere.

127 The other cases where parallel potentials act as a potential barrier are shown in Figure 3. In
128 this type, dynamical trajectories filled all velocity space in $v_{//}$, and parallel temperature (0.5
129 eV at the ionosphere) did not change above the ionosphere up to geosynchronous altitudes,
130 while perpendicular temperature decreased to 0.87 eV at 20,000 km, and to 0.42 eV at
131 geosynchronous altitudes. We conclude that accelerating potential raised parallel
132 temperature of the escaping ionospheric species. The potential barriers did not change the
133 parallel temperature of the ionospheric source.

134 A brief explanation is given below as to how the local potentials that have extracted electrons
135 and ions from the ionosphere developed at higher altitudes above the ionosphere. We note
136 that electrons and ions traveling earthward in the left-hand side of the velocity space marked
137 by Σ may contribute to the development of parallel potentials. In flux tubes where parallel
138 potential accelerates electrons (ions) out of the ionosphere, the same parallel potential in the
139 flux tubes acts as a potential barrier for ions (electrons) escaping ionosphere. In this flux tube
140 small pitch-angle electrons (ions) and large pitch-angle ions (electrons) traveling earthward
141 generate downward (upward) electric fields by charge separation along the flux tubes of
142 mirror geometry [Alfvén and Fälthammar, 1963; Persson, 1963; Stern, 1981]. These
143 potentials are global in scale and vary monotonically from ionosphere to the equator.
144 However, a rate of parallel potential change (parallel electric fields) may decrease above an
145 altitude of 10,000 km because magnetic mirror force drops rapidly in these regions.

146 The resultant potential distributions in the polar ionosphere and in the magnetosphere are
147 presented in Figure 4. Because of parallel potentials in the magnetosphere, potential
148 difference in the ionosphere never weakens but instead amplifies during equatorial projection.

149

150 *4. Field-aligned current*

151 Ions in the E layer drifted from positive potentials in higher latitudes to negative potentials in
152 lower latitudes to discharge imbalance produced by the mobility difference. Drift velocities of

153 these ions ($\mathbf{U}_{i\perp}$) may be given as,

154

$$\mathbf{u}_{i\perp} = \frac{\Omega_i}{B\nu_{in}} \mathbf{E}_p \quad (7)$$

155

Here, Ω_i , ν_{in} , \mathbf{E}_p denote ion cyclotron frequency, ion-neutral collision frequency and

156

secondary polarization electric fields, respectively. Substituting mean ion cyclotron and ion-

157

neutral collision frequencies in (7), we have ion drift velocities on the order of 5.9×10^1 m/s

158

for electric fields of the order of 0.1 V/m. Those drifting ions carry southward Pedersen

159

currents of the order of $1.0 \mu\text{A}/\text{m}^2$ in the E-layer. These ionospheric currents might be

160

redirected to the field-aligned currents at the poleward and equatorward edge of the flow

161

channel of the current to close 2-D current system. We therefore suggest that field-aligned

162

currents of the order of $1.0 \mu\text{A}/\text{m}^2$ may flow above the ionosphere in the ionospheric

163

injection scenario. To test this hypothesis, we calculate the field-aligned currents along the

164

dynamical trajectories using $\mathbf{J}_{\parallel q} = nq|e|\langle v_{\parallel} \rangle$, where

165

$$\langle v_{\parallel} \rangle = \frac{\int_{\Sigma} v_{\parallel} f(v) d^3v}{\int_{\Sigma} f(v) d^3v} \quad (8)$$

166

To calculate electric currents, velocity space integration was carried out only in the positive

167

velocity component in v_{\parallel} (traveling tailward), because those in negative velocity

168

component traveling earthward may be reflected in the magnetic mirror geometry and cancel

169

the earthward currents. The results show that ionospheric electrons at altitudes of 10,000 km

170

(electrostatic potential is 50 V) carry downward field-aligned currents of the order of

171

$2.0 \mu\text{A}/\text{m}^2$ at the number density $10^1 / \text{m}^3$. This is a fraction of the background density at

172

those altitudes ($n = 10^9 / \text{m}^3$). We conclude that upward flowing ionospheric electrons may

173

close Pedersen currents at the poleward edge of the channel, while upward flowing

174

ionospheric ions (oxygen ions) at the equatorward edge of the channel carried $0.69 \text{nA}/\text{m}^2$

175

at the same altitudes (electrostatic potential is -50 V) and same number density of electron

176

currents. Electric currents carried by the ions are smaller than those carried by electrons by

177

the mass ratio of electrons and ions if temperatures of electrons and ions are the same. They

178

cannot provide sufficient current density to close the Pedersen currents. Therefore, electrons

179

from the magnetosphere are necessary for closing the Pedersen currents at the equatorward

180 edge of the channel.

181

182 *5. Summary and Discussion*

183 Despite the ionospheric dynamo processes driven by the neutral wind, local electrostatic
184 fields that form in less than one minute may be expected in ionospheric injection because
185 electrons participate the dynamo process. Electrons are pumped up towards negative
186 electrodes in lower latitudes by ExB drift. The drift generates poleward Hall currents flowing
187 in an opposite direction in the equatorward electric field. The westward electric fields of the
188 magnetospheric origin may generate the ionospheric dynamo. The dynamo process yielded
189 plasma injections arising out of the ionosphere (evaporation of ionospheric plasmas) and
190 generated preferentially field-aligned potentials below 10,000 km.

191 Although the substorm onset would be triggered initially by the magnetospheric convection
192 enhancement (arrival of the Dipolarization Front from the tail), we suggest that activation of
193 the ionospheric dynamo (auroral onset) may be controlled by the intensity of westward
194 electric fields penetrating the auroral ionosphere. Because electric fields penetrating the
195 ionosphere are stronger in dark hemisphere (lower Pedersen conductance) than in sunlit
196 hemisphere (higher Pedersen conductance) [Saka, 2019], auroras are more active in the
197 dark hemisphere [Newell et al., 1996].

198 Field-aligned potentials were generated in the magnetosphere such that the ionospheric
199 potentials were amplified during their equatorial projection. This means that the ionosphere
200 responded to the initial dipolarization by returning the southward electric fields to the
201 dipolarization region in the magnetosphere. The southward electric fields in the ionosphere
202 that became earthward electric fields in the plasma sheet further displaced the dipolarizing
203 flux tube eastward which relaxed the radial inhomogeneity and intensified the dipolarization
204 [Saka, 2020]. This positive feedback loop may happen in the magnetosphere and ionosphere
205 systems with asymmetric development of the dipolarization region in dawn-dusk directions.
206 This asymmetry may be related to the difference in onset time of substorm current wedge in
207 dawn and dusk sectors [Nagai, 1991]. In this scenario, Harang Discontinuity (HD) is
208 generated in the auroral ionosphere through the ionospheric injection processes and
209 projected back to the magnetosphere to modify the existing magnetospheric convection
210 patterns [e.g., Artemyev et al., 2016]. This scenario differs from the proposal of [Erickson et
211 al., 1991; Liu and Rostoker, 1991] that asymmetric plasma pressure distribution introduced
212 in the equatorial plane of the nightside magnetosphere produced HD in the polar ionosphere.
213 It was suggested that a deformation velocity of aurora is about 5-8 km/s regardless of its
214 scale size [Oguti, 1975a, 1975b]. Oguti [1975b] noted from his observations that large-scale
215 auroras (~ 1000 km) such as bulge or surge are the sum of small-scale auroras (~3 km) such

216 as rays. Small-scale auroras that may be equivalent to the minimum size of the electrostatic
217 potential of negative charge are fundamental to the MI coupling processes in the ionospheric
218 injection scenario.

219
220

221 6. Data availability. No data sets were use in this article.

222

223 7. Competing interest. The author declares that there is no conflict of interest.

224

225

226

227 References

228

229 Alfvén, H. and Fälthammar, C.-G.: *Cosmical Electrodynamics*, 2nd ed., Oxford University
230 Press, New York, 1963.

231 Artemyev, A.V., Angelopoulos, A., Runov, A., and Zelenyi, L.M.: Earthward electric field and
232 its reversal in the near-Earth current sheet, *J. Geophys. Res.*, 121, 10803-10812,
233 doi:10.1002/2016JA023200, 2016.

234 Baker, D.N., Pulkkinen, T.I., Angelopoulos, V., Baumjohann, W., and McPherron, R.L.:
235 Neutral line model of substorms: Past results and present view, *J. Geophys. Res.*, 101,
236 12795-130010, 1996.

237 Birn, J., Hesse, M., Haerendel, G., Baumjohann, W., and Shiokawa, K: Flow braking and the
238 substorm current wedge, *Geophys. Res.*, 104, 19895-19903, 1999.

239 Birn, J., Raeder, J., Wang, Y.L., Wolf, R.A., and Hesse, M.: On the propagation of bubbles in
240 the geomagnetic tail, *Ann. Geophys.*, 22, 1773-1786, 2004.

241 Chiu, Y.T. and Schulz, M.: Self-consistent particle and parallel electrostatic field distributions
242 in the magnetospheric-ionospheric auroral region, *J. Geophys. Res.* 83, 629-642,
243 1978.

244 Erickson, G.M., Spiro, R.W., and Wolf, R.A.: The physics of the Harang discontinuity, *J.*
245 *Geophys. Res.*, 96, 1633-1645, 1991.

246 Liu, W.W., and Rostoker, G.: Effects of dawn-dusk pressure asymmetry on convection in the
247 central plasma sheet, *J. Geophys. Res.*, 96, 11501-11512, 1991.

248 Liu, W.W., and Liang, J.: Disruption of magnetospheric current sheet by quasi-electrostatic
249 field, *Ann. Geophys.*, 27, 1941-1950, 2009.

250 Liu, J., Angelopoulos, V., Zhou, X.-Z., and Runov, A.: Magnetic flux transport by dipolarizing
251 flux bundles, *J. Geophys. Res.*, 119, 909-926, doi:10.1002/2013JA019395, 2014.

252 Lui, A.T.Y.: Current disruption in the Earth's magnetosphere: Observations and models, J.
253 Geophys. Res., 101, 13067-13088, 1996.

254 McPherron, R.L., Russell, C.T., and Aubry, M.P.: Satellite studies of magnetospheric
255 substorms on August 15, 1968: 9. Phenomenological model for substorms, J.
256 Geophys. Res., 78, 3131-3148, 1973.

257 Nagai, T.: An empirical model of substorm-related magnetic field variations at synchronous
258 orbit, Magnetospheric substorms, Geophysical monograph 64, Edited by J.R. Kan,
259 T.A. Potemra, S. Kokubun, and T. Iijima, 91-95, 1991.

260 Newell, P.T., Meng, C.I., and Lyons, K.M.: Suppression of discrete aurorae by sunlight,
261 Nature, 381, 766-767, 1996.

262 Nielsen, E., and Greenwald, R.A.: Variations in ionospheric currents and electric fields in
263 association with absorption spikes during substorm expansion phase, J. Geophys.
264 Res., 83, 5645-5654, 1978.

265 Oguti, T.: Similarity between global auroral deformations in DAPP photographs and small
266 scale deformations observed by a TV camera, J. Atmos. Terr. Phys., 37, 1413-1418,
267 1975a.

268 Oguti, T.: Metamorphoses of aurora, Memoirs of NIPR, series A, 12, 1975b.

269 Persson, H.: Electric field along a magnetic line of force in a low-density plasma: Phys. Fluids,
270 6, 1756-1759, 1963.

271 Runov, A., Angelopoulos, V., Zhou, X.-Z., Zhang, X.-J., Li, S., Plaschke, F., and Bonnell, J.:
272 A THEMIS multicasestudy of dipolarization fronts in the magnetotail plasma sheet, J.
273 Geophys. Res., 116, A05216, doi:10.1029/2010JA016316, 2011.

274 Roux, A., Perraut, S., Robert, P., Morane, A., Pedersen, A., Korth, A., Kremser, G., Aparicio,
275 B., Rodgers, D., and Pellinen, R.: Plasma sheet instability related to the westward
276 traveling surge, J. Geophys. Res., 96, 17697-17714, 1991.

277 Saka, O., Hayashi, K, and Thomsen, M.: First 10 min intervals of Pi2 onset at
278 geosynchronous altitudes during the expansion of energetic ion regions in the
279 nighttime sector, J. Atmos. Solar Terr. Phys., 72, 1100-1109, 2010.

280 Saka, O.: A new scenario applying traffic flow analogy to poleward expansion of auroras, Ann.
281 Geophys., 37, 381-387, 2019.

282 Saka, O.: The increase in the curvature radius of geomagnetic field lines preceding a
283 classical dipolarization, Ann. Geophys., 38, 467-479, 2020.

284 Stern, D.P.: One-dimensional models of quasi-neutral parallel electric fields, J. Geophys.
285 Res., 86, 5839-5860, 1981.

286 Tanaka, T., Nakamizo, A., Yoshikawa, A., Fujita, S., Shinagawa, H., Shimazu, H., Kikuchi, T.,
287 and Hashimoto, K.: Substorm convection and current system deduced from the global

288 simulation, J. Geophys. Res., 115, A05220, doi:10.1029/2009JA014676, 2010.
289 Wahlund, J.-E., Opgenoorth, H.J., Haggstrom, I., Winsor, K.J., and Jones, G.O.: EISCAT
290 observations of topside ionospheric outflows during auroral activity: revisited,
291 J.Geophys.Res., 97, 3019-3017, 1992.

292

293

294

295

296

297

Figure captions

298

299 Figure 1.

300 A schematic illustration of the plasma injection arising out of dynamic ionosphere
301 (ionospheric injection). See text for detailed explanation.

302

303 Figure 2.

304 Regions of velocity space (Σ) occupied by the ionospheric species are shown. They were
305 accelerated by the parallel potentials and magnetic mirror force: (A) electrons (ions) at 1,000
306 km altitudes for parallel potentials of 10 V (-10 V), (B) electrons (ions) at 10,000 km for 50 V
307 (-50 V), (C) electrons (ions) at 20,000 km for 200 V (-200 V), and (D) electrons (ions) at
308 geosynchronous altitudes for 500 V (-500 V). In the velocity space, (v_{\parallel} , v_{\perp}) are normalized
309 by the thermal velocity of respective particles (1 eV for this case).

310

311 Figure 3.

312 Same as Figure 2 but parallel potential behaved as potential barriers: (A) electrons (ions) at
313 1,000 km for parallel potentials of -10 V (10 V), (B) electrons (ions) at 10,000 km for -50 V
314 (50 V), (C) electrons (ions) at 20,000 km for -200 V (200 V), and (D) electrons (ions) at
315 geosynchronous altitudes for -500 V (500 V).

316

317 Figure 4.

318 Equatorial projection of the ionospheric potentials (ϕ_i^+ and ϕ_i^-) from southern and northern
319 hemispheres is illustrated. Ionospheric potentials are positive in higher latitudes (ϕ_i^+) and

320 negative in lower latitudes (ϕ_i^-). Field-aligned potential amplified potential difference in the
321 ionosphere during the equatorial projection ($\phi_m^{++} > \phi_i^+$, $\phi_m^{--} < \phi_i^-$). Earthward electric fields
322 are produced in the plasma sheet.
323

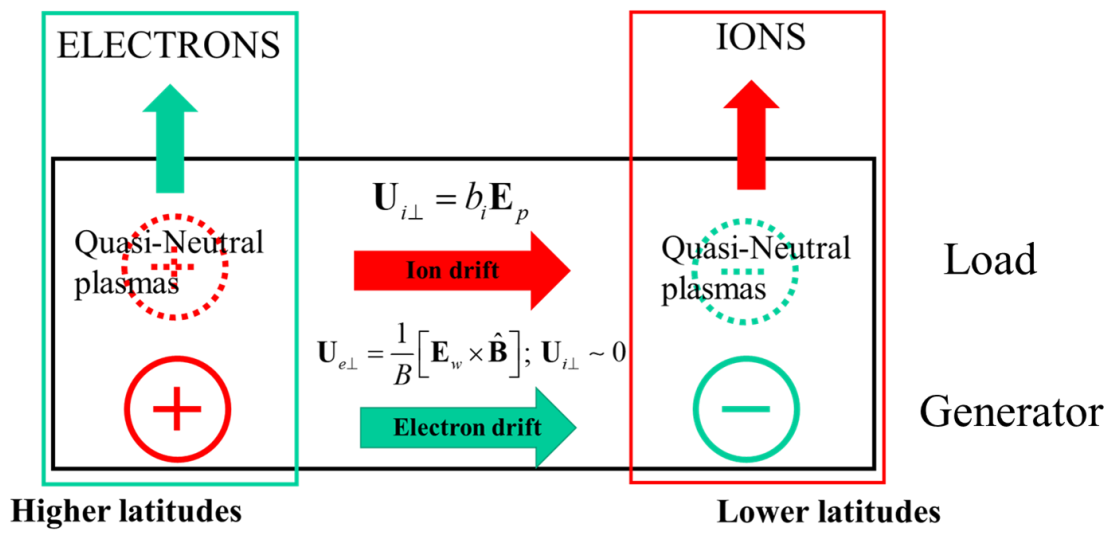


Figure 1

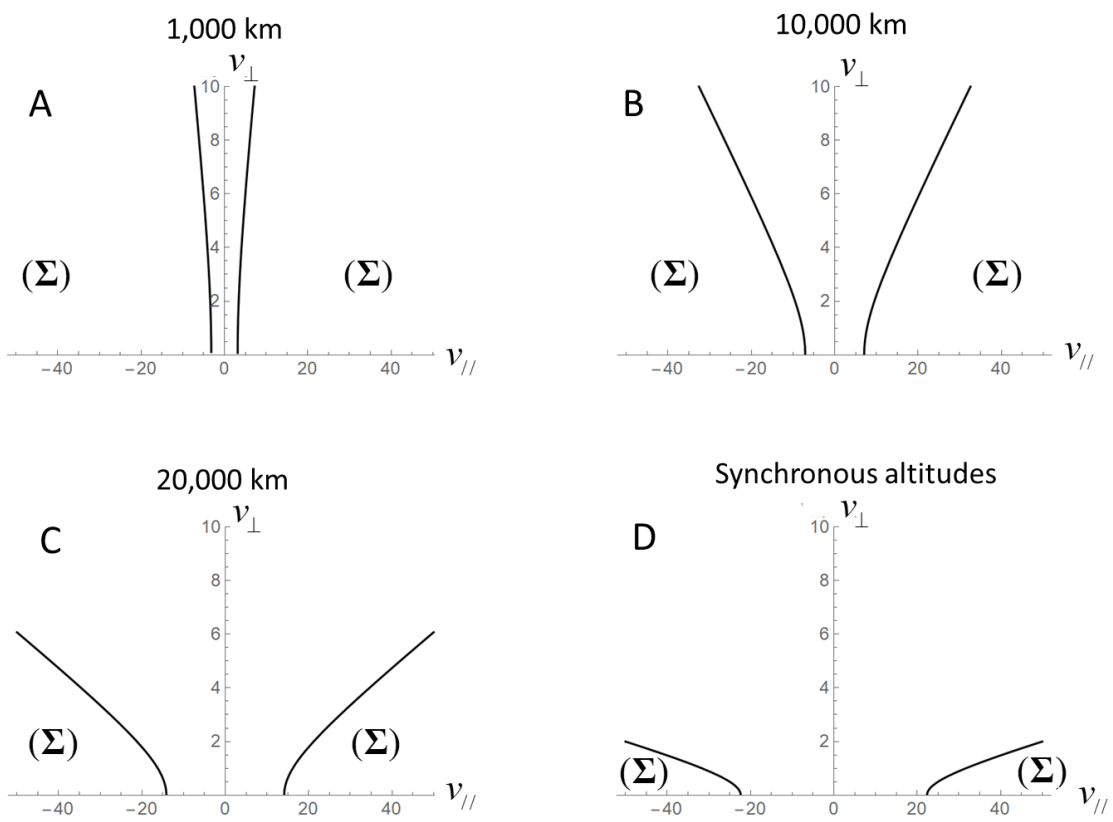


Figure 2

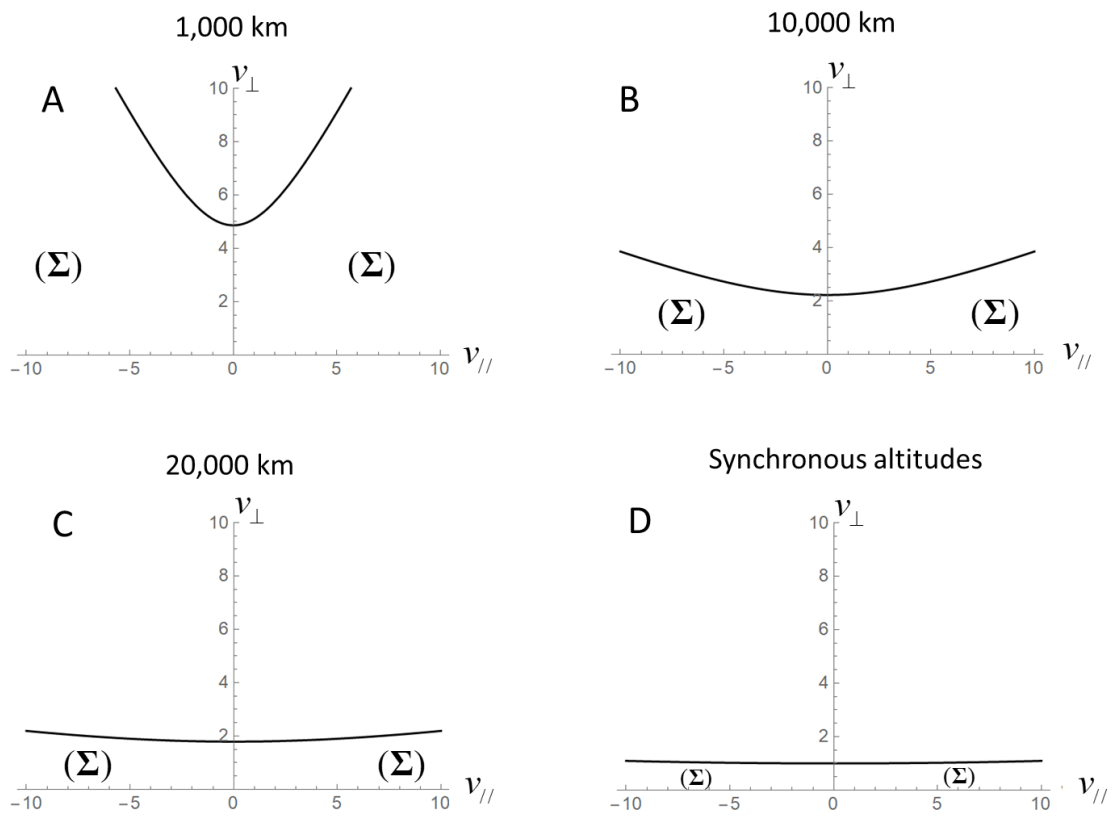


Figure 3

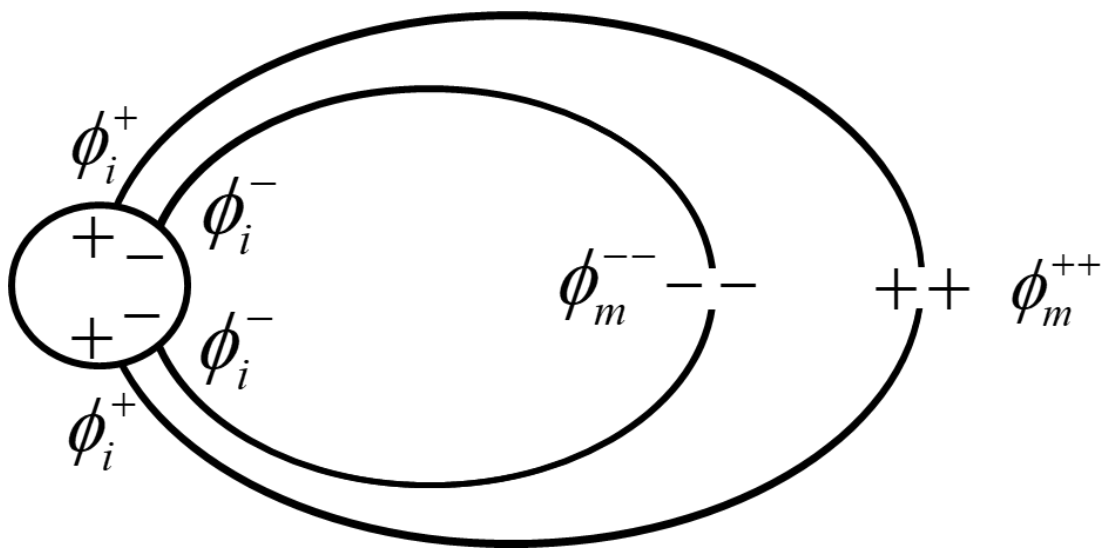


Figure 4